

Article

## Microbial Reducibility of Fe(III) Phases Associated with the Genesis of Iron Ore Caves in the Iron Quadrangle, Minas Gerais, Brazil

Ceth W. Parker <sup>1</sup>, Julie A. Wolf <sup>2</sup>, Augusto S. Auler <sup>3</sup>, Hazel A. Barton <sup>1,2</sup> and John M. Senko <sup>1,2,\*</sup>

<sup>1</sup> Department of Biology, The University of Akron, Akron, OH 44325-3908, USA;  
E-Mails: cwp13@zips.uakron.edu (C.W.P.); bartonh@uakron.edu (H.A.B.)

<sup>2</sup> Department of Geosciences, The University of Akron, Akron, OH 44325-4101, USA;  
E-Mail: jaw166@zips.uakron.edu

<sup>3</sup> Institute of Karst, Belo Horizonte, MG 30150-170, Brazil; E-Mail: aauler@gmail.com

\* Author to whom correspondence should be addressed; E-Mail: senko@uakron.edu;  
Tel.: +1-330-972-8047; Fax: +1-330-972-7611.

Received: 6 September 2013; in revised form: 2 November 2013 / Accepted: 15 November 2013 /

Published: 26 November 2013

**Abstract:** The iron mining regions of Brazil contain thousands of “iron ore caves” (IOCs) that form within Fe(III)-rich deposits. The mechanisms by which these IOCs form remain unclear, but the reductive dissolution of Fe(III) (hydr)oxides by Fe(III) reducing bacteria (FeRB) could provide a microbiological mechanism for their formation. We evaluated the susceptibility of Fe(III) deposits associated with these caves to reduction by the FeRB *Shewanella oneidensis* MR-1 to test this hypothesis. Canga, an Fe(III)-rich duricrust, contained poorly crystalline Fe(III) phases that were more susceptible to reduction than the Fe(III) (predominantly hematite) associated with banded iron formation (BIF), iron ore, and mine spoil. In all cases, the addition of a humic acid analogue enhanced Fe(III) reduction, presumably by shuttling electrons from *S. oneidensis* to Fe(III) phases. The particle size and quartz-Si content of the solids appeared to exert control on the rate and extent of Fe(III) reduction by *S. oneidensis*, with more bioreduction of Fe(III) associated with solid phases containing more quartz. Our results provide evidence that IOCs may be formed by the activities of Fe(III) reducing bacteria (FeRB), and the rate of this formation is dependent on the physicochemical and mineralogical characteristics of the Fe(III) phases of the surrounding rock.

**Keywords:** iron reducing bacteria; iron ore caves; biospeleogenesis; *Shewanella oneidensis* MR-1; canga; iron ore; banded iron formations

## 1. Introduction

Abundant karst-like features occur within Fe-rich substrate of the iron ore mining regions of Brazil (primarily the Carajás region in Pará and the “Iron Quadrangle” region in Minas Gerais). This includes over 3000 caves, referred to as “iron ore caves” (IOCs; Figure 1) [1,2]. The mechanisms of IOC formation in the relatively insoluble, Fe(III)-rich rocks of the region are poorly understood. Nonetheless, speleogenesis takes place in the broad geologic context of: (1) banded iron formations (BIFs), which are Precambrian sedimentary deposits composed predominantly of alternating layers of Fe(III) (hydr)oxides and chert or other non-Fe phases [3]; (2) ore-grade Fe deposits that form upon depletion of gangue minerals in BIFs (e.g., silica layers), giving rise to solids that are relatively enriched in Fe [4–6]; and (3) canga, which is a surficial breccia of weathered BIF and iron ore clasts that are cemented by secondary Fe(III) (hydr)oxides, and quite resistant to weathering processes [7,8]. The abundance of IOCs is rather unique to the Brazilian iron mining regions. Indeed, IOCs are rare in other major iron ore-producing regions of the world, such as the Lake Superior Iron Range and Sokoman Iron Formation of North America, the iron ore ranges of western Australia and South Africa, and the “Kursk Magnetic Anomaly” of Russia.

**Figure 1.** Interior of a cave adjacent to an Anglo American PLC mining site in Conceição do Mato Dentro CAI-03. Caver (standing, approximately 1.9 m tall) provided for scale. The cave passage is approximately 1 m tall.



It has been suggested that IOCs develop via the infiltration of fluids into BIF or iron ore underlying highly impermeable canga, leading to subsequent solubilization of Fe(III) (hydr)oxides in BIF or iron ore [predominantly hematite ( $\alpha$ -Fe<sub>2</sub>O<sub>3</sub>) in the Iron Quadrangle] [1,6,9,10]. However, itabirite substrates (containing BIF, canga, iron ore, and quartz) are very insoluble and have low erosion rates. Itabirite chemically weathers at rates between 2.37 and 2.69 m/Myr [11] and erodes at rates between 0.29 and 2.35 m/Myr [12]. Despite these low chemical weathering and erosion rates, high levels of dissolved Fe (up to 45  $\mu$ M) are seen in flowing waters and pools associated with the IOCs [13]. In the absence of reductive dissolution of Fe(III) phases hosting the caves, such high dissolved Fe concentrations appear unlikely. Thus, a purely abiotic mechanism for iron dissolution is unlikely.

Microorganisms with the ability to respire (leading to the reductive dissolution of) Fe(III) phases are widely distributed in the environment, and among phylogenetic lineages (e.g., [14,15]). While a microbial role in IOC formation has been suggested [16], no mechanism has been proposed. The role of microbiological activities in cave formation (biospeleogenesis) is becoming increasingly well-established, particularly with respect to sulfidic carbonate karst, where sulfuric acid speleogenesis is driven by sulfur oxidizing bacteria (e.g., [17–19]). IOCs do not form in carbonate-containing rocks [1,2], but we hypothesize a microbiological mechanism for the formation of IOCs, whereby Fe(III) reducing bacteria (FeRB) contribute to the reductive dissolution of Fe(III)-rich strata [13]. The organic carbon derived from the extensive surficial primary productivity of the Iron Quadrangle and Carajás regions of Brazil provides an abundant potential electron donor for FeRB to mobilize Fe as soluble Fe(II). Indeed, we have detected DOC concentrations as high as 57 mg/L in IOC-associated fluids [13], and using nucleic acid-based approaches to microbial community analysis, we have detected phylotypes attributable to evolutionary lineages of FeRB in IOCs. The biological reducibility of IOC-associated Fe(III) phases is implicit in the hypothesis that IOCs develop via the activities of FeRB. Fe(III) phases of varying characteristics (*i.e.*, mineralogy and Fe content) are present in these systems [6,9,10,20], which may exert considerable control on the susceptibility of the Fe(III) phases to reductive dissolution, and therefore cave formation. In this study, we collected various Fe(III)-rich phases from the Iron Quadrangle of Minas Gerais, Brazil where caves predominate, including BIF, iron ore, canga, and Fe(III)-rich samples (referred to as HEM<sub>spec</sub> and HEM<sub>lam</sub>) that were exposed during the mining process. We characterized the samples by differential chemical extractions, X-ray diffraction (XRD) analysis, and electron microscopy. In an effort to better constrain our model for biospeleogenesis in IOCs, we evaluated the susceptibility of these different Fe(III) phases to reductive dissolution by the FeRB *Shewanella oneidensis* MR-1.

## 2. Results and Discussion

### 2.1. Characterization of Fe(III)-Containing Phases

Collected canga and iron ore contained the highest total Fe content of the samples analyzed, while BIF and HEM<sub>lam</sub> contained relatively low total Fe contents (Table 1). The relatively high Fe content of canga is likely attributable to the fact that it is a secondary deposit of Fe(III) phases, and therefore, depleted in silica relative to BIF. Similarly, iron ore is likely derived from BIF that has been depleted of silica [3,7]. All solid phases contained minimal 0.5 M HCl-extractable Fe(II), illustrating that the Fe

in these sediments is predominantly Fe(III) (Table 1). Canga and iron ore contained the highest concentrations of hydroxylamine-HCl-extractable Fe(III), though in all cases, poorly crystalline Fe(III) comprised  $\leq 1\%$  of total Fe (Table 1), suggesting that the majority of Fe(III) is relatively crystalline [21].

**Table 1.** Fe contents of banded iron formation (BIF), canga, iron ore, and Fe(III)-rich material obtained from outwash of an iron ore cave (IOC) ( $\text{HEM}_{\text{spec}}$  and  $\text{HEM}_{\text{lam}}$ ). Fe(II), poorly-crystalline Fe(III), and total Fe are operationally defined based on extractability of Fe under conditions described in Experimental Section.

| Sample                     | Fe(II) ( $\mu\text{mol/g}$ ) | Poorly-crystalline Fe(III) ( $\mu\text{mol/g}$ ) | Total Fe ( $\text{mmol/g}$ ) |
|----------------------------|------------------------------|--|------------------------------|
| BIF                        | $1.37 \pm 0.10$              | $3.22 \pm 1.18$                                  | $1.79 \pm 0.17$              |
| Canga                      | $3.30 \pm 0.05$              | $12.54 \pm 5.32$                                 | $6.35 \pm 0.33$              |
| Iron Ore                   | $1.77 \pm 0.25$              | $24.37 \pm 5.28$                                 | $6.32 \pm 0.52$              |
| $\text{HEM}_{\text{spec}}$ | $1.77 \pm 1.02$              | $8.14 \pm 0.71$                                  | $2.19 \pm 0.61$              |
| $\text{HEM}_{\text{lam}}$  | $1.65 \pm 0.14$              | $3.65 \pm 1.14$                                  | $1.69 \pm 0.82$              |

Characterization of Fe-containing phases by XRD revealed that they contain abundant hematite and quartz, and in the case of canga, goethite (Figure 2). A lower peak to background ratio was also observed in the XRD pattern of canga in comparison to the other samples, which exhibited sharp peaks attributable to hematite and quartz (Figure 2). This suggested relatively poor crystallinity of canga-Fe(III), and is attributable to the abundance of secondary Fe(III) phases that cement BIF and/or iron ore clasts [7,8]. The most prominent peaks observed in the XRD patterns of BIF were attributable to quartz, with less prominent hematite peaks (Figure 2). XRD patterns of iron ore exhibited prominent peaks attributable to hematite, with less prominent quartz peaks (Figure 2). The difference in quartz signals between BIF and iron ore is likely a reflection of the mechanism of iron ore genesis, whereby silica is removed from BIF, giving rise to Fe-enriched material [3,5]. The XRD pattern of  $\text{HEM}_{\text{spec}}$  exhibited a more prominent pattern that matched hematite than  $\text{HEM}_{\text{lam}}$ , which exhibited a diffraction pattern dominated by quartz, with minor peaks attributable to hematite (Figure 2). These XRD results indicate that canga is distinct from the other Fe(III)-containing phases analyzed, being composed of relatively amorphous Fe(III) phases, as opposed to BIF, iron ore,  $\text{HEM}_{\text{spec}}$  and  $\text{HEM}_{\text{lam}}$ , which are composed of relatively crystalline quartz and hematite. These data also demonstrate that iron ore and  $\text{HEM}_{\text{spec}}$  are depleted in quartz compared to BIF and  $\text{HEM}_{\text{lam}}$  (Figure 2). Similarly, while energy dispersive X-ray spectroscopy (EDS)-based elemental mapping of solids revealed abundant Fe in all samples (Figure 3F–J), iron ore and  $\text{HEM}_{\text{spec}}$  contained lesser Si in comparison to BIF and  $\text{HEM}_{\text{lam}}$  (Figure 3K–O).

## 2.2. Extents and Rates of Fe(III) Bioreduction

We hypothesized that characteristics of Fe(III)-containing phases associated with IOCs would exert control on the susceptibility of those phases to reduction by the FeRB *S. oneidensis* MR-1. As such, we evaluated the dynamics of bioreduction of Fe(III) in BIF, canga, iron ore, and Fe(III)-rich waste material from mining operations ( $\text{HEM}_{\text{spec}}$  and  $\text{HEM}_{\text{lam}}$ ). *S. oneidensis* reduced Fe(III) in all samples to Fe(II) (Figure 4), but the extent of Fe(III) bioreduction did not exceed 3.37% of the total Fe(III) contained in the incubations (Table 2). The majority of Fe(III) bioreduction occurred within the first 9 days of incubation and extents of Fe(III) bioreduction [as indicated by maximal Fe(II) accumulation]

followed the pattern of canga > BIF > HEM<sub>lam</sub> > HEM<sub>spec</sub> > iron ore (Table 2, Figure 4A). We calculated first-order rate constants ( $k$ ) for Fe(III) bioreduction using the equation:

$$\ln[\text{Fe(III)}_{\text{tot}} - \text{Fe(II)}_t] = -kt + \ln[\text{Fe(III)}_{\text{tot}}] \quad (1)$$

where  $\text{Fe(III)}_{\text{tot}}$  is the total Fe(III) concentration, and  $\text{Fe(II)}_t$  is the Fe(II) concentration at a given time ( $t$ ).

**Figure 2.** X-ray diffraction patterns of BIF, canga, iron ore, and materials from the outwash of an IOC (HEM<sub>spec</sub> and HEM<sub>lam</sub>) that were collected in the Iron Quadrangle region of Brazil. All intensities were normalized based on the maximum intensity of each sample. Reference diffraction patterns of goethite, quartz, and hematite are shown for comparison and were generated using data from The American Mineralogist Crystal Structure Database [22].

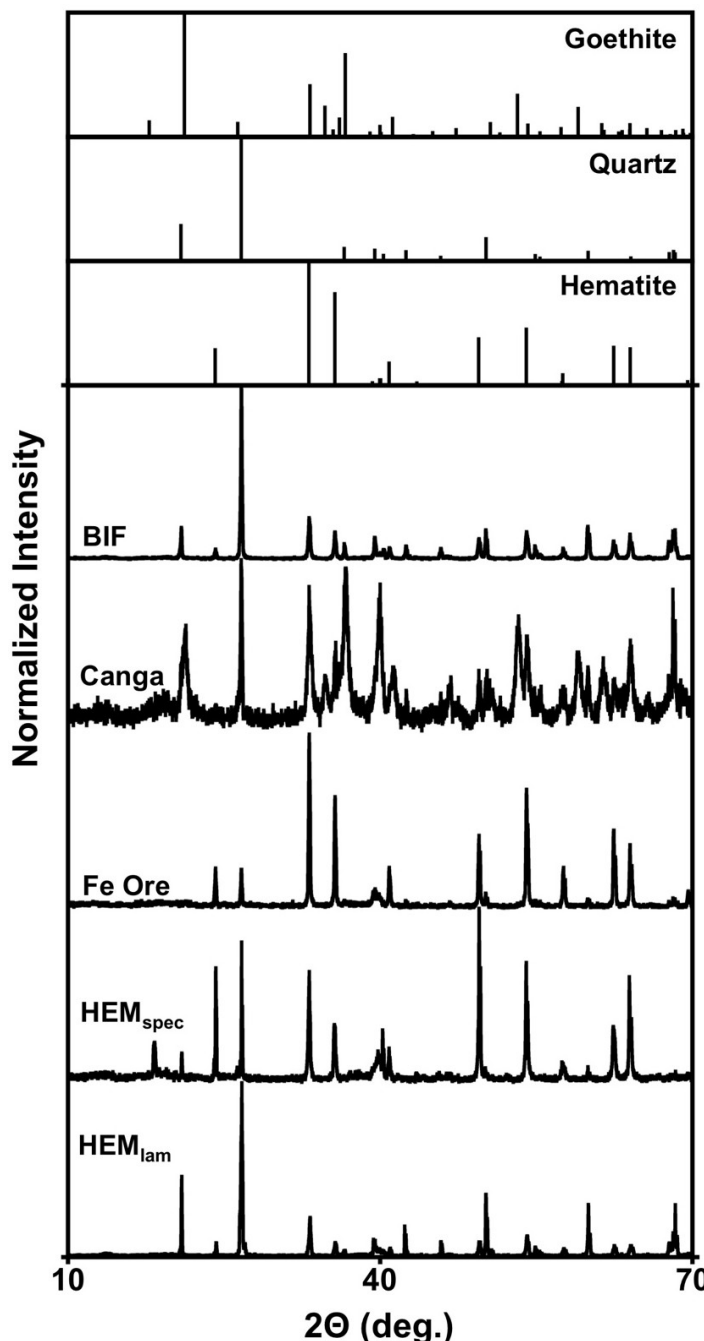


**Figure 3.** Scanning electron micrographs [panels (A)–(E)] and energy dispersive X-ray spectroscopy (EDS)-based maps of Fe [panels (F)–(J)] and Si [panels (K)–(O)] of BIF [panels (A), (F) and (K)], canga [(B), (G) and (L)], iron ore [panels (C), (H) and (M)], HEM<sub>spec</sub> [panels (D), (I) and (N)], and HEM<sub>lam</sub> [panels (E), (J) and (O)] used for bioreduction experiments. Scale bars = 40  $\mu$ m.

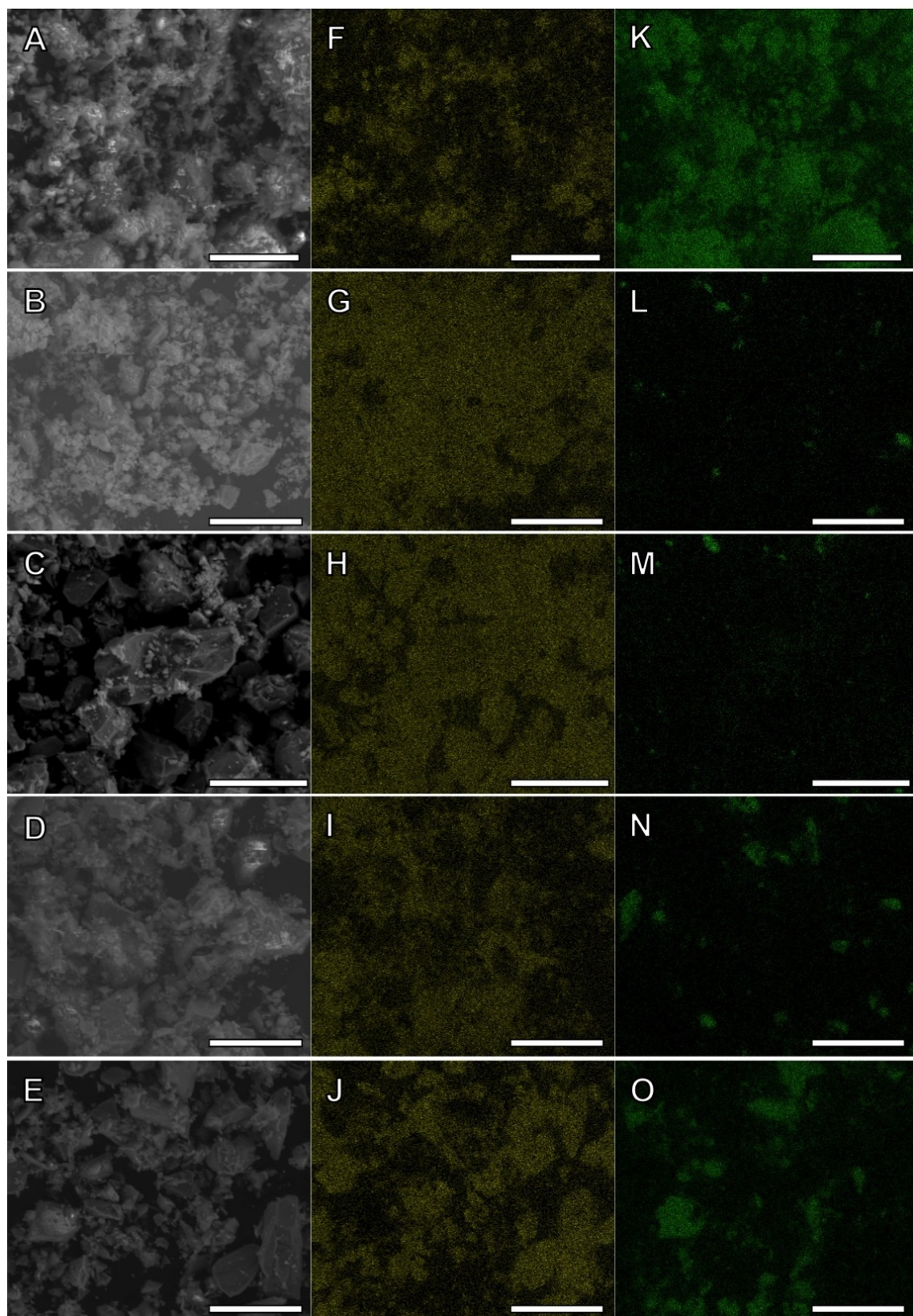


**Figure 4.** Total (0.5 M HCl-extractable) Fe(II) [(A) and (B)], soluble Fe(II) [(C) and (D)], and solid-associated Fe(II) [(E) and (F)] in incubations containing *S. oneidensis* MR-1 and BIF (●), canga (○), iron ore (■), material from HEM<sub>spec</sub> (□), and material from HEM<sub>lam</sub> (◆). Fe(II) concentrations in anthroquinone-2,6-disulfonate (AQDS)-free incubations are shown in panels (A), (C), and (E), and Fe(II) concentrations in AQDS-amended incubations are shown in panels (B), (D), and (F). Dashed lines represent respective Fe(II) concentrations in uninoculated incubations. Error bars represent one standard deviation.

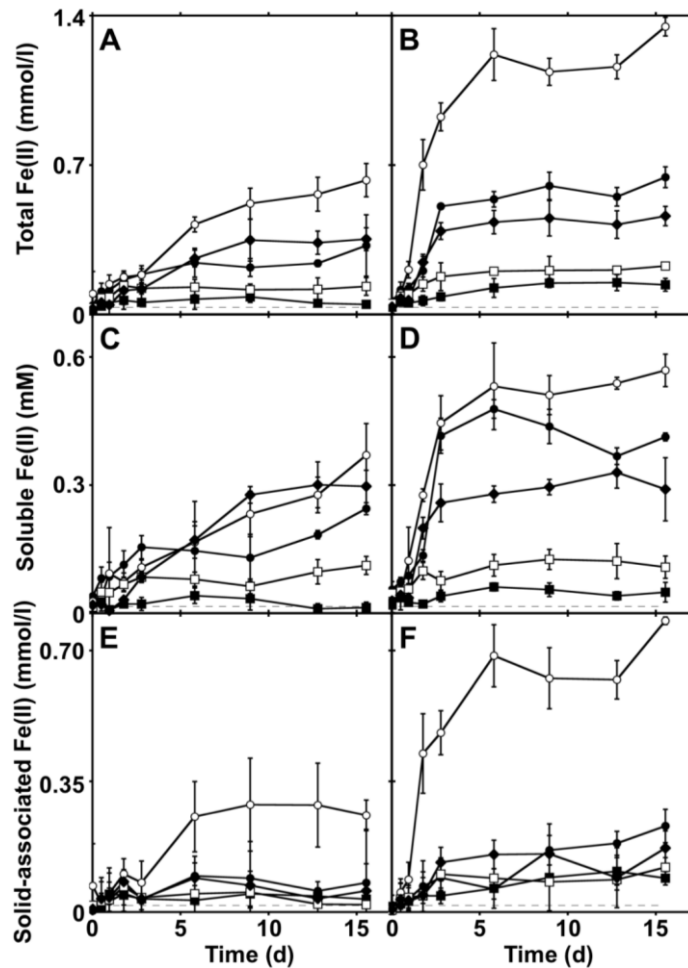


**Table 2.** Rates and extents of Fe(III) bioreduction in incubations containing *S. oneidensis* MR-1 and Fe(III)-containing phases.

| Sample              | Fe(III) reduction $k$ (day $^{-1}$ ) |          | Total Fe(III) reduced (%) |          | Hydroxylamine-HCl-extractable Fe(III) reduced (%) |          |
|---------------------|--------------------------------------|----------|---------------------------|----------|---|----------|
|                     | (-) AQDS                             | (+) AQDS | (-) AQDS                  | (+) AQDS | (-) AQDS  | (+) AQDS |
| BIF                 | 0.0012                               | 0.0039   | 0.81                      | 1.61     | 450   | 894      |
| Canga               | 0.0013                               | 0.0089   | 1.57                      | 3.37     | 797   | 1707     |
| Iron Ore            | 0.0007                               | 0.0004   | 0.21                      | 0.37     | 27  | 49       |
| HEM <sub>spec</sub> | 0.0008                               | 0.0011   | 0.34                      | 0.57     | 91  | 153      |
| HEM <sub>lam</sub>  | 0.0009                               | 0.0034   | 0.88                      | 1.15     | 409   | 534      |

Notes: % total Fe(III) reduced = [maximum total Fe(II) measured/total Fe(III) in incubation]  $\times$  100;  
% hydroxylamine-extractable Fe(III) reduced = [maximum total Fe(II) measured/hydroxylamine-extractable Fe(III) in incubation]  $\times$  100.

While the kinetics of Fe(III) bioreduction are controlled by a variety of complex factors, including Fe(III) surface area, Fe(III) surface structure, and Fe(II) adsorption onto Fe(III) phases and cells [23–25], we chose a relatively simple first order rate formulation for the purpose of comparing rates of Fe(III) bioreduction among a variety of Fe(III) phases. Initial rates of Fe(III) bioreduction exhibited a similar trend to the observed extents of Fe(III) reduction, with canga- and BIF-Fe(III) undergoing reduction at the greatest initial rates, while iron ore- and HEM<sub>spec</sub>-Fe(III) underwent bioreduction at the lowest initial rates.

The rate and extent of canga-associated Fe(III) bioreduction were greater than for any of the other Fe(III) containing phases (Figure 4A, Table 2). This is attributable to the relatively poor crystallinity of canga-associated Fe(III) in comparison to the other phases, where the dominant Fe(III) phase was hematite (Figure 2). Generally hematite is quite resistant to bioreduction compared to amorphous Fe(III) phases such as ferrihydrite and hydrous ferric oxide (HFO), due to thermodynamic, particle size, and surface chemical considerations [26]. Indeed, iron ore, which exhibited the strongest hematite signal by XRD (Figure 2), was the least susceptible to bioreduction (Figure 4A). Material from HEM<sub>spec</sub>, which exhibited a similarly strong hematite signal in analysis by XRD, was slightly more susceptible to bioreduction than iron ore (Figure 4A), while Fe(III) associated with BIF and HEM<sub>lam</sub> was more susceptible to bioreduction than either iron ore or HEM<sub>spec</sub> material (Figure 4A). The amount of hydroxylamine-HCl-extractable Fe(III) associated with sediments is routinely used as an indicator of the amount of bioreducible Fe(III) (mostly as HFO and/or ferrihydrite) [21]. While a relatively minor amount of the total Fe(III) associated with the solid phases could be reduced by *S. oneidensis*, the amount of Fe(III) associated with canga, BIF, and HEM<sub>lam</sub> exceeded the amount of hydroxylamine-HCl extractable Fe(III) (Table 2), suggesting that crystalline Fe(III) associated with the solid phases was susceptible to partial bioreduction. The extent of bioreduction of Fe(III) associated with iron ore and HEM<sub>spec</sub> was less than the amount of hydroxylamine-HCl extractable Fe(III) (Table 2). This suggests that crystalline Fe(III) associated with these solids was not susceptible to bioreduction, and/or a fraction of the poorly crystalline Fe(III) could not be reduced. The relatively low extents of Fe(III) reduction are consistent with previous work indicating the poor bioreducibility of hematite. In these experiments, conducted under similar conditions with *Shewanella* species, <5% of synthetic hematite was reduced [26–31]. Nonetheless, mineralogical identity of the Fe(III) phase is not the sole determinant of the extent of Fe(III) bioreduction, as nearly 10% of Fe(III) in a naturally occurring Eatontown hematite was susceptible to bioreduction by a *Shewanella* species [26].

### 2.3. Enhancement of Fe(III) Bioreduction by an Electron Shuttling Compound

Soils of humid tropical savannas such as the *Cerrado* in which the Iron Quadrangle is located contain high levels of soil organic carbon, which may influence microbial Fe(III) reduction [32,33]. Soil organic carbon may enhance microbial Fe(III) reduction by serving as an electron donor to support Fe(III) reduction, as well as acting as a ligand to limit adsorption of biogenic Fe(II) on Fe(III) phases, thus limiting surface passivation of Fe(III) bioreduction [27,28]. Additionally, redox-active organic molecules, such as humic substances, serve to shuttle electrons from microorganisms to Fe(III) [34–36]. Under this scenario, organic molecules serve as respiratory electron acceptors, and subsequently transfer electrons to insoluble Fe(III) phases. This electron shuttle-dependent strategy of

microbial Fe(III) reduction may enhance the overall extent of Fe(III) reduction, as it allows the transfer of electrons to surfaces in small pores of Fe(III) phases that would otherwise be inaccessible to attachment of microbial cells and direct transfer of electrons to the Fe(III) phase [34–37].

We evaluated the bioreduction of Fe(III) phases by *S. oneidensis* MR-1 in the presence of anthroquinone-2,6-disulfonate (AQDS), as an electron shuttling analogue of humic substances [35,36]. The addition of AQDS to incubations led to greater extents of Fe(III) bioreduction in all cases, and maximum extents of Fe(III) reduction for each Fe(III)-containing phase followed the same trend as AQDS-free incubations, with canga > BIF > HEM<sub>lam</sub> > HEM<sub>spec</sub> > iron ore (Figure 4A,B, Table 2). The addition of AQDS to incubations led to reduction of Fe(III) in excess of the poorly crystalline Fe(III) content of the solids (Table 2), suggesting that relatively crystalline phases were susceptible to bioreduction. Nonetheless, a fraction of poorly crystalline Fe(III) associated with iron ore remained resistant to reduction (Table 2). An examination of the initial rates of Fe(III) bioreduction demonstrates that the addition of AQDS to the incubations enhanced the Fe(III) bioreduction rate, except for iron ore-associated Fe(III) (Table 1). These results suggest that the presence of complex organic matter may enhance the bioreduction of Fe(III) phases associated with the Iron Quadrangle.

#### 2.4. Controls on Fe(III) Bioreduction

The relatively high rates and extents of canga-Fe(III) bioreduction can be attributed to the poor crystallinity of the Fe(III) found in canga, whereas crystalline Fe(III) phases, such as those found in the iron ore, are generally more resistant to bioreduction (e.g., [21,26,38–40]). Examination of canga solids by scanning electron microscopy (SEM) revealed smaller Fe(III)-rich particles than the other solids (Figure 3A–E), which would also enhance Fe(III) bioreduction [23,25,41]. Iron ore contained large particles (many  $\geq 10 \mu\text{m}$ ) that were not observed in other solid phases (Figure 3A–E), while particles in BIF were of similar sizes and morphologies to those in canga (Figure 3A,B). The particles in HEM<sub>spec</sub> and HEM<sub>lam</sub> exhibited similar sizes and morphologies to each other as well (Figure 3D,E). As a result, mineralogy and surface area of the solids can not completely explain the variability in rates and extents of bioreduction of Fe(III) associated with the various Fe(III)-rich phases (Figure 4A,B), especially as crystalline hematite was the predominant Fe(III) phase detected by XRD in all of these samples (Figure 2). Substitutions of chemical species (notably Al) within mineral matrices may modulate the bioreducibility of Fe(III) phases [42,43], though the effect of Al substitution on bioreduction appears to vary, depending on the mineralogy of the Fe(III) phases [44]. However, after preliminary examination of the Fe(III) phases by Mössbauer spectrometry we were unable to detect evidence of differences in Al substitution (data not shown).

While more crystalline, and more thermodynamically stable Fe(III) (hydr)oxides (e.g., goethite or hematite) are generally less susceptible to bioreduction than amorphous Fe(III) phases (e.g., HFO or ferrihydrite), thermodynamic explanations for the incomplete reduction of Fe(III) (hydr)oxides do not appear to completely predict extents of Fe(III) reduction [40]. Rather, accumulation of biogenic Fe(II) on Fe(III) (hydr)oxide surfaces, which is partially influenced by Fe(III) (hydr)oxide surface area, appears to be a major limiting factor in the extent of Fe(III) bioreduction [40]. Adsorption of Fe(II) on Fe(III) phases and cell surfaces leads to passivation of further Fe(III) reducing reactions, but binding of biogenic Fe(II) to soluble or insoluble ligands may alleviate this inhibition [27,28,45]. Notably, work

by Urrutia *et al.* [45] illustrated that non-bioreducible solid phases (alumina or clays in [45]) could act as “Fe(II) sinks” to which Fe(II) could adsorb. Adsorption of Fe(II) onto Fe(II) sinks limits its adsorption onto Fe(III) (hydr)oxide and/or cell surfaces, thus enhancing the bioreduction of crystalline Fe(III) phases [45]. Sasowsky *et al.* [46] also demonstrated that the presence of quartz in mixed systems promoted removal of dissolved iron from solution. While biogenic soluble Fe(II) was variable among the incubations (Figure 4C,D) and contributed to the variability in extents of Fe(III) bioreduction (Figure 4A,B), solid associated Fe(II) was consistent among BIF, iron ore, HEM<sub>spec</sub> and HEM<sub>lam</sub> (Figure 4E,F). BIF-Fe(III) and HEM<sub>lam</sub>-Fe(III) were more susceptible to reduction and exhibited stronger quartz signals and Si abundances than iron ore and HEM<sub>spec</sub> (Figures 1, 2 and 4). These findings suggest that quartz may have served as an Fe(II) sink in the incubations, limiting Fe(II)-induced passivation of Fe(III) bioreduction.

## 2.5. Implications for the Role of FeRB in IOC Formation

The results that we present here illustrate the variability in the rate and extent of bioreduction of Fe(III) associated with different formations involved in IOC speleogenesis in the Brazilian Iron Quadrangle. Fe(III) associated with all phases was susceptible to at least partial bioreduction, indicating a potential role for FeRB in the formation of IOCs. The variable rates of Fe(III) bioreduction suggest that rates of IOC formation, if biogenic in origin, could be similarly variable and dependent on the mineralogy and quartz content of the phases that are undergoing reductive dissolution. An implication of this is that IOCs would be formed at greater rates in rocks hosting Fe(III) phases that are more susceptible to reductive dissolution (*i.e.*, canga). Caves in canga or at the interface between canga and BIF/iron ore represent the majority of IOCs recorded in Brazil [47]. Canga is a much younger rock than BIF, which might imply shorter timescales for speleogenesis [3,8]. Thus, IOCs in canga may evolve faster due to the higher susceptibility of canga-Fe(III) to bioreduction, as we have demonstrated here. However, we point out that *in situ* rates of Fe(III) bioreduction, regardless of Fe(III) phase characteristics, may vary, depending on hydraulic characteristics and extents of biogenic Fe(II) adsorption.

While BIF/iron ore-Fe(III) is more resistant to bioreduction than canga-Fe(III), IOC formation at the interface between canga and BIF/iron ore may be facilitated by groundwater flow at this interface. Canga is highly resistant to physical erosion on its surface, and often demonstrates lower permeability relative to underlying BIF/iron ore strata. As a result, BIF/iron ore experience extensive water circulation and associated weathering, especially in the Iron Quadrangle, which receives approximately 1.5 m/year of rain [6–8]. This hydrologic flow may enhance Fe(III) bioreduction by delivering organic electron donor and nutrients to support FeRB activities [48], while exporting biogenic Fe(II), and consequently alleviating Fe(II)-induced inhibition of Fe(III) reduction [48–50]. Indeed, while complete bioreductive dissolution of crystalline Fe(III) phases is rarely observed in batch incubations, nearly complete reduction of goethite ( $\alpha$ -FeOOH) was achieved in continuous-flow columns inoculated with the FeRB *S. putrefaciens* CN32 [51].

We propose that IOCs may be at least partially formed by biospeleogenesis, whereby FeRB mediate the reductive dissolution of Fe(III) phases [13]. This microbial activity coupled with the hydraulic export of soluble biogenic Fe(II) leads to increased porosity of the Fe(III) containing strata, and

ultimately cave formation. This mechanism of biospeleogenesis may be considered analogous to carbonate-hosted sulfidic caves, in that microbiological activities lead to the chemical dissolution of rock, with subsequent hydraulic export of now-dissolved constituents of the rock [13]. In the cases of carbonate-hosted caves, speleogenesis will generally continue as long as acidic water is delivered to the rock, but this may not be the case with IOCs. Under the proposed scenario, reductive dissolution of Fe(III) phases leads to increased porosity and export of Fe from the subsurface. However, this increased porosity would also enhance intrusion of O<sub>2</sub> into the IOC voids, limiting further Fe(III) reduction and speleogenesis. The self-limiting mechanism that we propose may explain why IOCs are generally smaller than carbonate-hosted caves [1,2]. Additionally, biospeleogenesis of IOCs may provide a mechanism for formation of canga, which may be a result of reductive mobilization of Fe from BIF or iron ore. Canga features have been proposed to result from the influx of aqueous Fe(II), which was subsequently oxidized by atmospheric O<sub>2</sub>, and the resulting Fe(III) (hydr)oxides cemented larger rock fragments [1]. Microbially-mediated reductive dissolution of BIF/iron ore-associated Fe(III) coupled with hydrologic transport of biogenic Fe(II) is a potential mechanism for the mobilization of aqueous Fe that would be required for canga formation.

### 3. Experimental Section

#### 3.1. Sample Collection

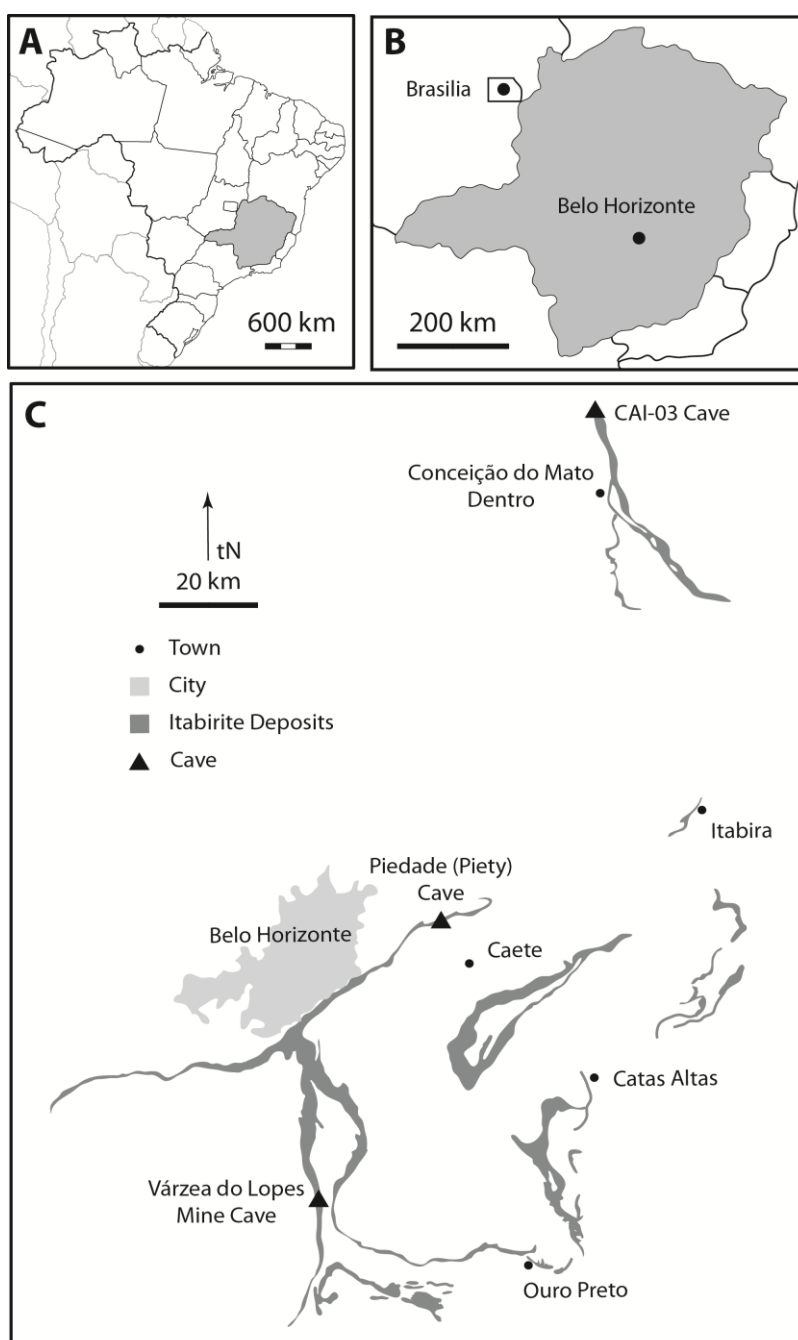
All samples were collected in the Iron Quadrangle region of Minas Gerais, Brazil. BIF and canga samples were collected from rubble near the Piedade (Piety) Cave in Caeté, Minas Gerais, Brazil (Figure 5). Iron ore samples were collected from the Várzea do Lopes open pit mine operated by Gerdau, S.A. in the municipality of Itabirito, Minas Gerais, Brazil (Figure 5). Fluids associated with the iron ore samples had a pH of 7.2. Samples were also collected from a stream flowing out of a cave adjacent to an Anglo American PLC mining site in Conceição do Mato Dentro CAI-03 (Figure 5). These latter samples were likely exposed by blasting during mining, and are referred to as HEM<sub>spec</sub>, and HEM<sub>lam</sub>. HEM<sub>spec</sub> had a shiny, metallic lustre like specular hematite, and HEM<sub>lam</sub> was laminated, brittle, and friable. BIF and canga samples were broken with a rock hammer to recover pieces of approximately 1 cm<sup>3</sup>. All samples were ground to a fine powder in a ball mill before further processing and analysis.

#### 3.2. Characterization of Fe Phases

Fe(II), poorly crystalline Fe(III), and total Fe were operationally defined as Fe that could be extracted from the solids using 0.5 M HCl [Fe(II)], 0.25 M hydroxylamine in 0.25 M HCl [poorly crystalline Fe(III)], and concentrated HNO<sub>3</sub> followed by concentrated HCl (total Fe) [21]. After the solubilization steps, undigested solids were removed by centrifugation and Fe in the supernatant was quantified. Fe(II) that was extracted from solids using 0.5 M HCl and 0.25 M hydroxylamine in 0.25 M HCl was quantified by ferrozine assay [52]. Dissolved Fe after extraction of total Fe was determined by atomic absorption spectrometry (AAS; PerkinElmer AAnalyst 700; Waltham, MA, USA). All samples were characterized by powder X-ray diffraction (XRD) analysis and scanning electron microscopy (SEM). Samples for XRD were packed in aluminum sample holders and analysis was carried out using

a Phillips 3100 automated diffractometer using CuK $\alpha$  radiation scanning at  $2\Theta$  of  $2^\circ$  to  $70^\circ$ , and an accelerating voltage of 40 kV at 35 mA. Intensities were measured with a  $0.02^\circ$  step size at one second intensity-counting time per step. Mineral phases present in samples were identified by comparison of sample diffraction patterns to reference diffraction patterns. For microscopic and elemental characterization of solid phases, samples were mounted on aluminum stubs with two-sided tape and examined by SEM using and FEI (FEI Company, Hillsboro, OR, USA) Quanta 200 Environmental Scanning Electron Microscope fitted with an EDAX (EDAX Inc., Draper, UT, USA) energy dispersive X-ray spectroscopy (EDS) system for determination of elemental composition of solids.

**Figure 5.** Map showing locations of caves and sampling locations from this study. Map of Brazil (A) with Minas Gerais shaded. Panel (B) illustrates location of Belo Horizonte. And panel (C) illustrates sampling locations and itabirite deposits in relation to Belo Horizonte.



### 3.3. Bioreduction Incubations

Experiments to assess the bioreducibility of Fe(III)-containing phases were conducted in a solution containing 20 mM sodium lactate, vitamins and trace metals [53], and buffered (pH 7) with 20 mM 4-(2-hydroxyethyl)-1-piperazineethanesulfonic acid (HEPES). Different autoclaved Fe(III)-containing phases were added to incubation solutions from concentrated stock suspensions to achieve total Fe concentrations of 40 mmol/L. Where appropriate, anthroquinone-2,6-disulfonate (AQDS) was added to incubations to achieve a concentration of 20 µM. All incubations were conducted in sealed serum bottles under an O<sub>2</sub>-free headspace of 97% N<sub>2</sub> and 3% H<sub>2</sub>. *S. oneidensis* MR-1 cells were cultured aerobically in trypticase soy broth without dextrose to late log phase, and harvested by centrifugation. Cells were washed three times in the anoxic HEPES-buffered solution described above. Cells were resuspended in the same solution and added to Fe(III)-containing incubations to achieve cell concentrations of approximately  $7 \times 10^7$  cells/mL in each serum bottle. Incubations that received *S. oneidensis* MR-1 were conducted in triplicate, and uninoculated incubations that served as negative controls were conducted in duplicate. All incubations were carried out at 25 °C in darkness. Samples were periodically removed from the incubations and soluble Fe(II) and total Fe(II) were quantified. In preparation for quantification of soluble Fe(II), solids were removed from the suspensions by centrifugation, the supernatant was removed and acidified with 0.5 M HCl, and Fe(II) was quantified by ferrozine assay [52]. Total Fe(II) was extracted from solids in 0.5 M HCl, solids were removed from the suspensions by centrifugation, and Fe(II) was quantified by ferrozine assay [52].

## 4. Conclusions

The results that we present here provide evidence that a biospeleogenesis model may be applied to the formation of IOCs in the iron ore mining regions of Brazil. Under the model that we propose, FeRB mediate the reductive dissolution of Fe(III) phases associated with BIF, canga, and iron ore formations, with subsequent export of aqueous Fe(II). These activities may be enhanced by the locally high primary productivity (providing abundant organic electron donor for Fe(III) reduction and electron shuttling compounds) and high extents of subsurface water circulation, both of which would enhance reductive dissolution of Fe(III) required for IOC biospeleogenesis.

## Acknowledgments

This work was supported by the Instituto do Carste and UA startup funds to H.A.B. The authors gratefully acknowledge Anglo American PLC and Gerdau, S.A. for allowing access to caves near their mining operations. We thank Ira Sasowsky (Department of Geosciences, The University of Akron) for his suggestions during manuscript preparation. SEM was performed at The University of Akron Environmental Scanning Electron Microscopy Laboratory, which was created with the support of NSF EAR grant 0320898.

## Conflicts of Interest

The authors declare no conflict of interest.

## References

1. Simmons, G.C. Canga caves in the Quadrilátero Ferrífero, Minas Gerais, Brazil. *Bull. Nat. Speleol. Soc.* **1963**, *25*, 66–72.
2. Auler, A.; Farrant, A.R. A brief introduction to karst and caves in Brazil. *Proc. Univ. Bristol Spelaeol. Soc.* **1996**, *20*, 187–200.
3. Bekker, A.; Slack, J.F.; Planavsky, N.; Krapež, B.; Hoffmann, A.; Konhauser, K.O.; Rouxel, O.J. Iron formation: The sedimentary product of a complex interplay among mantle, tectonic, oceanic, and biospheric processes. *Econ. Geol.* **2010**, *105*, 467–508.
4. Morris, R.C.; Thornber, M.R.; Ewer, W.E. Deep-seated iron ores from banded-iron formation. *Nature* **1980**, *288*, 250–252.
5. Morris, R.C. A textural and mineralogical study of the relationship between iron ore to banded-iron formation in the Hamersley iron province of Western Australia. *Econ. Geol.* **1980**, *75*, 184–209.
6. Varajão, C.A.C.; Bruand, A.; Ramanaidou, E.R.; Gilkes, R.J. Microporosity of BIF hosted hematite ore, Iron Quadrangle, Brazil. *An. Acad. Bras. Ciênc.* **2002**, *74*, 113–126.
7. Harder, E.C. The “itabirite” iron ores of Brazil. *Econ. Geol.* **1914**, *9*, 101–111.
8. Schuster, D.L.; Farley, K.A.; Vasconcelos, P.M.; Balco, G.; Monteiro, H.S.; Waltenberg, K.; Stone, J.O. Cosmogenic  $^3\text{He}$  in hematite and goethite from Brazilian “canga” duricrust demonstrates the extreme stability of these surfaces. *Earth Planet. Sci. Lett.* **2012**, *329–330*, 41–50.
9. Rosière, C.A.; Siemes, H.; Quade, H.; Brokmeier, H.-G.; Jansen, E.M. Microstructures, textures, and deformation mechanisms in hematite. *J. Struct. Geol.* **2001**, *23*, 1429–1440.
10. Guedes, S.C.; Rosière, C.A.; Barley, M.E. The association of carbonate alteration of banded iron formation with the Carajás high-grade hematite deposits. *Appl. Earth Sci.* **2003**, *112*, 26–30.
11. Salgado, A.A.R.; Braucher, R.; Colin, F.; Nalini, H.A.; Varajão, A.F.D.C.; Varajão, C.A.C. Denudation rates of the Quadrilátero Ferrífero (Minas Gerais, Brazil): Preliminary results from measurements of solute fluxes in rivers and *in situ*-produced cosmogenic  $^{10}\text{Be}$ . *J. Geochem. Explor.* **2006**, *88*, 313–317.
12. Salgado, A.A.R.; Braucher, R.; Varajão, A.C.; Colin, F.; Varajão, A.F.D.C.; Nalini, H.A. Relief evolution of the Quadrilátero Ferrífero (Minas Gerais, Brazil) by means of ( $^{10}\text{Be}$ ) cosmogenic nuclei. *Z. Geomorphol.* **2008**, *52*, 317–323.
13. Parker, C.W.; Auler, A.S.; Senko, J.M.; Sasowsky, I.D.; Piló, L.B.; Smith, M.; Johnston, M.; Barton, H.A. Microbial Iron Cycling and Biospeleogenesis: Cave Development in the Carajás Formation, Brazil. In Proceedings of the 16th International Congress of Speleology, Brno, Czech Republic, 21–27 July 2013; Filippi, M., Bosák, P., Eds.; Czech Speleological Society: Praha, Czech Republic, 2013; pp. 442–446.
14. Lovley, D.R.; Holmes, D.E.; Nevin, K.P. Dissimilatory Fe(III) and Mn(IV) reduction. *Adv. Microb. Physiol.* **2004**, *49*, 219–286.
15. Weber, K.A.; Achenbach, L.A.; Coates, J.D. Microorganisms pumping iron: Anaerobic microbial iron oxidation and reduction. *Nat. Rev. Microbiol.* **2006**, *4*, 752–764.

16. McFarlane, M.J.; Twidale, C.R. Karstic features associated with tropical weathering profiles. *Z. Geomorphol. Suppl.* **1987**, *64*, 73–95.
17. Barton, H.A.; Luiszer, F. Microbial metabolic structure in a sulfidic cave hot spring: Potential mechanisms of biospeleogenesis. *J. Cave Karst Stud.* **2005**, *67*, 28–38.
18. Engel, A.S. Microbial Diversity of Cave Ecosystems. In *Geomicrobiology: Molecular and Environmental Perspectives*; Barton, L.L., Mandl, M., Loy, A., Eds.; Springer: New York, NY, USA, 2010; pp. 219–238.
19. Barton, H.A. Biospeleogenesis. In *Treatise on Geomorphology*; Shroder, J.F., Ed.; Academic Press: San Diego, CA, USA, 2013; Volume 6, pp. 39–55.
20. Spier, C.A.; Barros de Oliveira, S.M.; Rosière, C.A.; Ardisson, J.D. Mineralogy and trace-element geochemistry of the high-grade iron ores of the Águas Claras Mine and comparison with the Capão Xavier and Tamaduá iron ore deposits, Quadrilátero Ferrífero, Brazil. *Miner. Deposita* **2008**, *43*, 229–254.
21. Lovley, D.R.; Phillips, E.J.P. Rapid assay for microbially reducible ferric iron in aquatic sediments. *Appl. Environ. Microbiol.* **1987**, *53*, 1536–1540.
22. Downs, R.T.; Hall-Wallace, M. The American Mineralogist crystal structure database. *Am. Mineral.* **2003**, *88*, 247–250.
23. Burgos, W.D.; Royer, R.A.; Fang, Y.; Yeh, G.-T.; Fisher, A.S.; Jeon, B.-H.; Dempsey, B.A. Theoretical and experimental considerations related to reaction-based modeling: A case study using iron(III) oxide bioreduction. *Geomicrobiol. J.* **2002**, *19*, 253–287.
24. Neal, A.L.; Rosso, K.M.; Geesey, G.G.; Gorby, Y.A.; Little, B.J. Surface structure effects on direct reduction of iron oxides by *Shewanella oneidensis*. *Geochim. Cosmochim. Acta.* **2003**, *67*, 4489–4503.
25. Bose, S.; Hochella, M.F., Jr.; Gorby, Y.A.; Kennedy, D.W.; McCready, D.E.; Madden, A.S.; Lower, B.H. Bioreduction of hematite nanoparticles by the dissimilatory iron reducing bacterium *Shewanella oneidensis* MR-1. *Geochim. Cosmochim. Acta.* **2009**, *73*, 962–976.
26. Zachara, J.M.; Fredrickson, J.K.; Li, S.-M.; Kennedy, D.W.; Smith, S.C.; Gassman, P.L. Bacterial reduction of crystalline Fe<sup>3+</sup> oxides in single phase suspensions and subsurface materials. *Am. Mineral.* **1998**, *83*, 1426–1443.
27. Royer, R.A.; Burgos, W.D.; Fisher, A.S.; Unz, R.F.; Dempsey, B.A. Enhancement of biological reduction of hematite by electron shuttling and Fe(II) complexation. *Environ. Sci. Technol.* **2002**, *36*, 1939–1946.
28. Royer, R.A.; Burgos, W.D.; Fisher, A.S.; Jeon, B.H.; Unz, R.F.; Dempsey, B.A. Enhancement of hematite bioreduction by natural organic matter. *Environ. Sci. Technol.* **2002**, *36*, 2897–2904.
29. Royer, R.A.; Dempsey, B.A.; Jeon, B.-H.; Burgos, W.D. Inhibition of biological reductive dissolution of hematite by ferrous iron. *Environ. Sci. Technol.* **2004**, *38*, 187–193.
30. Stone, J.J.; Royer, R.A.; Dempsey, B.A.; Burgos, W.D. Effect of natural organic matter on zinc inhibition of hematite bioreduction by *Shewanella putrefaciens* CN32. *Environ. Sci. Technol.* **2007**, *41*, 5284–5290.
31. Luan, F.; Burgos, W.D.; Xie, L.; Zhou, Q. Bioreduction of nitrobenzene, natural organic matter, and hematite by *Shewanella putrefaciens* CN32. *Environ. Sci. Technol.* **2010**, *44*, 184–190.

32. Jobbágy, E.G.; Jackson, R.B. The vertical distribution of soil organic carbon and its relation to climate and vegetation. *Ecol. Appl.* **2000**, *10*, 423–436.
33. Zinn, Y.L.; Resck, D.V.S.; da Silva, J.E. Soil organic carbon as affected by afforestation with *Eucalyptus* and *Pinus* in the *Cerrado* region of Brazil. *For. Ecol. Manage.* **2002**, *166*, 285–294.
34. Lovley, D.R.; Coates, J.D.; Blunt-Harris, E.L.; Phillips, E.J.P.; Woodward, J.C. Humic substances as electron acceptors for microbial respiration. *Nature* **1996**, *382*, 445–448.
35. Fredrickson, J.K.; Zachara, J.M.; Kennedy, D.W.; Dong, H.; Onstott, T.C.; Hinman, N.W.; Li, S. Biogenic iron mineralization accompanying the dissimilatory reduction of hydrous ferric oxide by a groundwater bacterium. *Geochim. Cosmochim. Acta* **1998**, *62*, 3239–3257.
36. Scott, D.T.; McKnight, D.M.; Blunt-Harris, E.L.; Kolesar, S.E.; Lovley, D.R. Quinone moieties act as electron acceptors in the reduction of humic substances by humics-reducing microorganisms. *Environ. Sci. Technol.* **1998**, *32*, 2984–2989.
37. Zhang, C.; Liu, C.; Shi, Z. Micromodel investigation of transport effects on the kinetics of reductive dissolution of hematite. *Environ. Sci. Technol.* **2013**, *47*, 4131–4139.
38. Lovley, D.R.; Phillips, E.J.P. Availability of ferric iron for microbial reduction in bottom sediments of the freshwater tidal Potomac River. *Appl. Environ. Microbiol.* **1986**, *52*, 751–757.
39. Lovley, D.R.; Phillips, E.J.P. Novel mode of microbial energy metabolism: organic carbon oxidation coupled to dissimilatory reduction of iron or manganese. *Appl. Environ. Microbiol.* **1988**, *54*, 1472–1480.
40. Dominik, P.; Kaupenjohann, M. Reduction of Fe(III) (hydr)oxides with known thermodynamic stability by *Geobacter metallireducens*. *Geomicrobiol. J.* **2004**, *21*, 287–295.
41. Roden, E.E.; Zachara, J.M. Microbial reduction of crystalline iron(III) oxides: Influence of oxide surface area and potential for cell growth. *Environ. Sci. Technol.* **1996**, *30*, 1618–1628.
42. Kukkadapu, R.K.; Zachara, J.M.; Smith, S.C.; Fredrickson, J.K.; Liu, C. Dissimilatory bacterial reduction of Al-substituted goethite in subsurface sediments. *Geochim. Cosmochim. Acta* **2001**, *65*, 2913–2924.
43. Dominik, P.; Pohl, H.N.; Bousserrhine, N.; Berthelin, J.; Kauperjohann, M. Limitations to the reductive dissolution of Al-substituted goethites by *Clostridium butyricum*. *Soil Biol. Biochem.* **2002**, *34*, 1147–1155.
44. Ekstrom, E.B.; Learman, D.R.; Madden, A.S.; Hansel, C.M. Contrasting effects of Al substitutions on microbial reduction of Fe(III) (hydr)oxides. *Geochim. Cosmochim. Acta* **2010**, *74*, 7086–7099.
45. Urrutia, M.M.; Roden, E.E.; Zachara, J.M. Influence of aqueous and solid-phase Fe(II) complexants on microbial reduction of crystalline iron(III) oxides. *Environ. Sci. Technol.* **1999**, *33*, 4022–4028.
46. Sasowsky, I.D.; Foos, A.; Miller, C.M. Lithic controls on the removal of iron and remediation of acidic mine drainage. *Water Res.* **2000**, *34*, 2742–2746.
47. Piló, L.B.; Auler, A. Geoespeleologia das Cavernas em Rochas Ferríferas da Região de Carajás, Pa. Sociedade Brasileira de Espeleologia (in Portuguese). In Proceedings of the Anais do 30th Congresso Brasileiro de Espeleologia, Montes Claros, MG, Brazil, 9–12 July 2009.
48. Minyard, M.L.; Burgos, W.D. Hydrologic flow controls on biologic iron(III) reduction in natural sediments. *Environ. Sci. Technol.* **2007**, *41*, 1218–1224.

49. Roden, E.E.; Urrutia, M.M. Ferrous iron removal promotes microbial reduction of crystalline iron(III) oxides. *Environ. Sci. Technol.* **1999**, *33*, 1847–1853.
50. Gonzalez-Gil, G.; Amonette, J.E.; Romine, M.F.; Gorby, Y.A.; Geesey, G.G. Bioreduction of natural specular hematite under flow conditions. *Geochim. Cosmochim. Acta.* **2005**, *69*, 1145–1155.
51. Roden, E.E.; Urrutia, M.M.; Mann, C.J. Bacterial reductive dissolution of crystalline Fe(III) oxide in continuous-flow column reactors. *Appl. Environ. Microbiol.* **2000**, *66*, 1062–1065.
52. Stookey, L.L. Ferrozine—A new spectrophotometric reagent for iron. *Anal. Chem.* **1970**, *42*, 779–781.
53. Tanner, R.S. Cultivation of Bacteria and Fungi. In *Manual of Environmental Microbiology*; Hurst, C.J., Knudsen, G.R., McInerney, M.J., Stetzenbach, L.D., Walter, M.V., Eds.; ASM Press: Washington, DC, USA, 1997; pp. 52–60.

© 2013 by the authors; licensee MDPI, Basel, Switzerland. This article is an open access article distributed under the terms and conditions of the Creative Commons Attribution license (<http://creativecommons.org/licenses/by/3.0/>).